Int. J. Electrochem. Sci., 15 **(2020)** 1996 – 2012, doi: 10.20964/2020.03.01

International Journal of
ELECTROCHEMICAL
SCIENCE
www.electrochemsci.org

Study on the Effect of F^- and Cl^- on the Differentiation of 904L Stainless Steel Passive Film in acid Environment

Xiaoqing Feng [1,2], *Wei Shi* [1,2], *Xuhong Chen* [3],*and Song Xiang* [1,2,*]

[1] College of Materials and Metallurgy, Guizhou University, Guiyang 550025, China;
[2] Key Laboratory for Mechanical Behavior and Microstructure of Materials of Guizhou Province, Guizhou University, Guiyang 550025, China
[3] Institute of Metrology and quality Inspection of Chongqing, Chongqing 401123, China;
[*]E-mail: sxiang@gzu.edu.cn

Received: 5 October 2019 / *Accepted:* 3 December 2019 / *Published:* 10 February 2020

In the field of metal corrosion, understanding the corrosive mechanism of corrosive ions on metals is very important for the protection of materials. In this paper, the effect of F^- and Cl^- on the corrosion of 904L stainless steel surface passive film in an acidic environment was studied. A comparison was made between how two ions form and destroy the passive film on a 904L stainless steel surface. Electrochemical dynamic behavior was studied by using cyclic polarization, potentiostatic polarization, electrochemical impedance spectroscopy (EIS), and so on. Selective solubilization was studied by an inductively coupled plasma optical emission spectrometer (ICP-OES) and the constitution of surface product films was analyzed by X-ray photoelectron spectroscopy (XPS). The results show that the F^- participate in the composition of the passive film formed by 904L in the F^--containing acidic environment.

Keywords: 904L stainless steel; cyclic polarization; passive film; F^-; Cl^-

1. INTRODUCTION

Hydrofluoric acid is a widely used acidic solution which is highly corrosive. Thus, polymeric materials (such as polytetrafluoroethylene) are generally used in the HF industry instead of metal. However, in the mineral-processing industry, the contact between metal and HF is inevitable. Ores containing impurities (such as CaF_2) are dissolved in concentrated sulfuric acid to form hydrofluoric acid, leading an $HF–H_2SO_4$ mixed acid environment. Fluorine and chlorine are of the same main group and have similar chemical properties. Various aspects of the corrosion behavior of Cl^- with metals have been studied extensively, forming a relatively complete system [1–4]. However it is still unclear whether there is a difference between the corrosion behavior of metals when exposed to F^- and Cl^-, respectively.

Polytetrafluoroethylene materials are commonly used in the fluorine industry, which has meant that the corrosion behavior of related metals in the fluorine environment are rarely studied; however from the rarity of literature, it was found that F^- has some properties: F^- and Ni react preferential reaction to form an insoluble layer; F^- has a chaotropic character; and F^- has a significant selective dissolution effect on iron. Zou et al. [5] have shown that HF preferentially reacts with Ni on 904L stainless steel to form a layer of insoluble deposits that hinder the formation of passivation films and destroy the integrity of the passive film, leading to more serious corrosion. Trompette et al. [6,7] have categorized anions based on their kosmotropic/chaotropic character. If the anion can fully approach the surface of the passive film and lose its hydration shell, the Cl^- can rupture the passive film at moderate potential, and pits will appear on the surface of the sample, whereas the F^- will not lead to pits. Li et al. [8] have shown that, when adding different concentrations of F^- in dilute acid solution, a high concentration of F^- leads to selective dissolution of Fe and accelerates corrosion, and fluoride ions participate in the composition of the oxide film.

The 904L has good corrosion resistance in sulfuric acidic environment [9]. Compared with 316L, 904L exhibits higher resistance to corrosion of acidic solution due to its higher Cr and Mo contents [9]. A heat exchanger made of 904L stainless steel has been used in the environments of mineral processing for many years, and it has been established that it can work normally during maintenance periods. However, its service life still needs to be improved. Therefore, it is very important to explore the influence mechanism of metals when exposed to the fluoride ion on 904L stainless steel and explore ways to improve its corrosion resistance.

In this paper, 904L was selected as the material for HF and HCl. The initial corrosion behavior of 904L when exposed to F^- and Cl^- acid solutions in different concentrations were compared. We discussed the effect of the structure, properties and corrosion resistance on 904L passive film by F^- and Cl^-.

2. MATERIALS AND METHODS

First, AISI 904L was used as the experimental material, and its elemental composition (wt%) is show in Table 1. We cut the sample (Φ15mm×6mm) from the plate of hot rolled and ground with it grits SiC paper from 320# to 2000#, then it was mirror polished, and cleaned with acetone, ethanol, and distilled water in an ultrasonic cleaner.

Table 1. Elemental composition of 904Lss (wt%).

Elements	**Cr**	**Ni**	**Mo**	**Mn**	**Cu**	**C**	**Si**	**S**	**N**	**P**	**Fe**
904L	19.68	24.08	4.293	1.470	1.273	0.016	0.292	=<0.15	0.084	0.027	Bal

The solutions used in the experiments were 0.01–0.05 mol/L HCl and HF solutions, and all experiments were carried out at (25 ± 0.1) °C.

The materials were all tested on the CS350 electrochemical workstation (CorrTest, Wuhan, China). The test used a three-electrode cell system, 904Lss sample as the working electrode and a flat platinum plate as a counter electrode, and a special Pt/PtO_2 was used as a reference electrode [10]. The scanning range of the potentiodynamic polarization curve is (versus open circuit potential (OCP)) between –0.2 and 1.5 V, and the scanning rate are 1 mv/s. The cyclic polarization curve was recorded from a versus OCP of –0.3 V, with a scan rate of 0.167 mV/s and retrace when the anodic polarization current reached 0.125 mV/cm^2. The potentiostatic measurements were performed at a constant anodic potential of +0.8V (Pt) for 1 h. Electrochemical impedance spectroscopy (EIS) measurements were employed at a voltage excitation amplitude of 10 mv and a scanning frequency range of 100 kHz to 10 mHz. The polarization and EIS test results were fitted using CView 2 and ZView 2, respectively. Each experiment was performed at least three times to determine the repeatability of the experimental data.

The corrosion morphology of the specimen, which was immersed in a 0.05 mol/L HCl and HF solution for seven days at (25 ± 0.1) °C on a material surface, was examined by scanning electron microscope (SEM).

X-ray photoelectron spectroscopy (XPS) was employed to examine the specimen after 7 days' exposure to the test solution. The XPS analysis was performed with a model ESCALAB 250Xi (ThermoFisher, Massachusetts, America) using a monochromized AlKα radiation source of 14.866 keV, 15 mA. Wide scans were acquired at 100 eV pass energy from 1350 to 0eV binding energy (BE), and regional scans were acquired through photoelectron regions of interest at 30eV pass energy. The binding energy was referenced to the C_{1s} 285 eV. We use XPSPeak to process data.

3. RESULTS AND DISCUSSION

3.1. Potentiodynamic polarization curve

The potentiodynamic polarization curves of 904L in HF and HCl solutions with different concentrations are shown in Fig. 1. A typical large passivation region of –0.5~0.3 V is proposed. This is due to the elemental composition of the 904L stainless steel, which is rich in Ni, Cr, and Mo [11]. Notably, an increase in F^- and Cl^- ion concentration in the solution leads to a shift in the corrosion potential and breakdown potential values toward the negative side, which indicated that the corrosion resistance of the sample decreases as the concentration increases.

The fitting results of corrosion potential (E_{corr}) and corrosion current density (I_{corr}) all polarization curves were obtained by Tafel extrapolation; passive current density (i_{pass}) and breakdown potential (E_b) are also tabulated in Table 2. The polarization curves of different concentrations of F^- and Cl^--containing acidic solutions in Fig.1 display similar trends.

In Fig. 1a, the E_b and E_{corr} decrease with the increasing of the solution concentration, the I_{corr} and i_{pass} increase synchronously with the increase in solution concentration, and the electrochemical parameters are more obvious with a change in the solution concentration. As shown in Fig. 1b, however, as the solution concentration increases, the change in electrochemical parameters is small, and the curves are also more concentrated. It can be seen that 904L was more sensitive to F^- than Cl^-.

Based on the above finding, the 904L passivation film is significantly affected by F^- and the composition has been noticeably changed in the F^--containing acidic solution.

Indeed, in the 0.01–0.05 mol/L HF solutions, the i_{pass} increased from 7.19 μA•cm^{-2} to 13.07 μA•cm^{-2}, and the E_b decreased from 388.19 mV to 225.85 mV. In the 0.01–0.05 mol/L HCl solutions, the i_{pass} increased from 2.84 μA•cm^{-2} to 4.36 μA•cm^{-2}, and the E_b decreased from 414.04 mV to 325.19 mV. This suggests that as the solution concentration increases, the tendency of pitting corrosion increases [12], and the E_{corr} in the F^--containing acid solution is lower than that of the Cl^--containing acidic solution at the same concentration, whereas the I_{corr} is higher than that of the Cl^--containing acidic solution, which means, F^- is more aggressive than Cl^- at the same concentration.

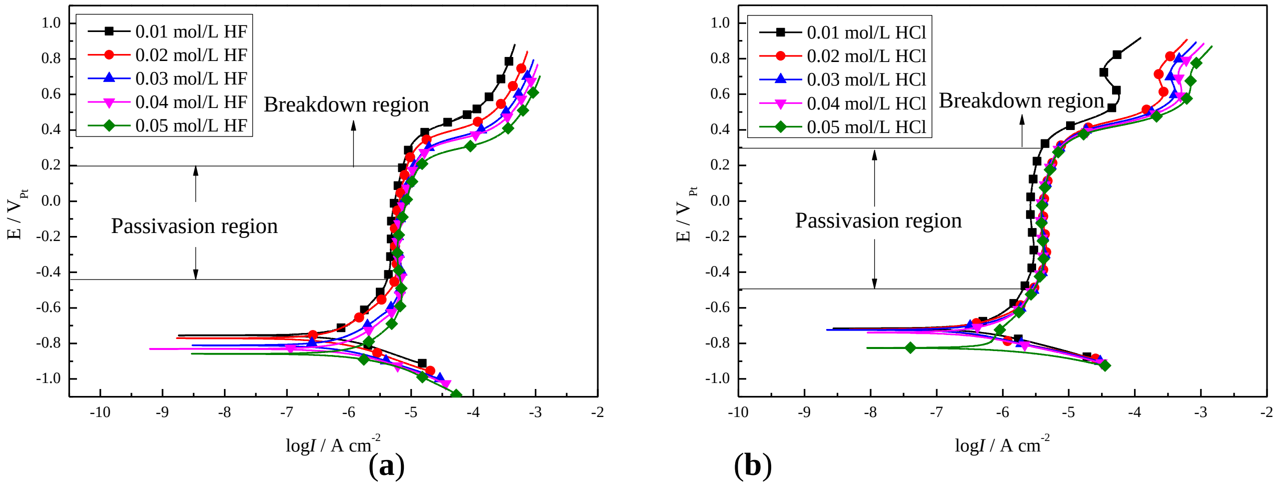

Figure 1. Potentiondynamic curves of 904L stainless steels in the 0.01–0.05 mol/L (a) HF, and (b) HCl solution.

Table 2. Results analyzed from polarization curves.

		I_{corr} (μA cm^{-2})	E_{corr} (mV)	E_b (mV)	i_{pass} (μA cm^{-2})	Corrosion Rate (μm/a)
HF	0.01 mol/L	0.59±0.02	–754±5	388±12	7.20±0.1	6.95±0.24
	0.02 mol/L	0.62±0.03	–771±15	341±8	8.40±0.3	7.34±0.35
	0.03 mol/L	0.76±0.03	–811±10	285±10	10.79±0.2	8.88±0.35
	0.04 mol/L	0.77±0.02	–831±12	277±7	10.92±0.3	9.09±0.24
	0.05 mol/L	1.94±0.05	–859±15	226±5	13.07±0.8	22.87±0.59
HCl	0.01 mol/L	0.13±0.01	–716±6	414±11	2.84±0.1	1.49±0.12
	0.02 mol/L	0.28±0.02	–721±9	348±10	3.92±0.1	3.35±0.24
	0.03 mol/L	0.41±0.03	–724±12	341±8	3.97±0.2	4.78±0.35
	0.04 mol/L	0.44±0.03	–739±11	333±4	4.11±0.3	5.16±0.35
	0.05 mol/L	0.99±0.04	–826±15	325±2	4.36±0.3	11.69±0.47

3.2. Electrochemical impedance analysis

We use the Electrochemical impedance spectroscopy to measure the relative stability of the passive films formed on 904L in the test solutions after open circuit potential is stable. Fig. 2a,b is presented as a Nyquist diagram, in which the capacitor arc corresponds to the interaction of the electric double layer capacitor and the metal dissolution. The charge transfer resistance at the metal / solution interface can be reflected by the capacitor arc diameter [13,14].

From the Bode diagram of the two solutions (Fig. 2c,d), log|Z| shows a linear relationship with log *f*, which is observed in the frequency range of 10^{-2} to 10^{1} Hz in the HF solution and 10^{-2} to 10^{2} Hz in the HCl solution, respectively. Since the two slopes are less than -1, the passive film behaves as a pseudocapacitive nature [15,16], and at the low frequencies appears a maximum of phase angle, indicating a capacitive-like behavior [17], and the maximum phase angle is less than 90 ° (~ 80 °) and the absolute value of the slope of the impedance modulus is lower than unity (～0.8) indicate a deviation of the ideal capacitor, usually due to dispersion of the time constant caused by the irregular surface of the electrode and the surface roughness [18]. In the higher frequency range (between 10^{4} and 10^{5} Hz of Fig. 2d), the phase angle in the Bode diagram approaches 0 ° and is almost independent of frequency, representing the electrolyte resistance [19]. Furthermore, there is only one time constant in the phase angle and frequency diagram. It can be seen that the polarization resistance is the value of |Z| at 0.01 Hz in the Bode diagram, which reflects the corrosion resistance of the 904L in the solution [16]. As show in Fig. 2c,d, the values of |Z| at 0.01 Hz for the HF solution (70–100 $\mathrm{K\Omega \cdot cm^{-2}}$) is lower than those of the HCl solution (100–200 $\mathrm{K\Omega \cdot cm^{-2}}$). It indicates that the passive film formed in the HCl solution and has good corrosion resistance. The different composition and thickness of the passive films formed by immersion in the HF and HCl solution, leading to the different corrosion resistance [16,17].

The equivalent circuit was used to fit the impedance data as shown in Fig. 2a [20]. The data obtained by fitting are listed in Table 3, where R_p represents the polarization resistance, R_s represents the solution resistance, and CPE represents the constant phase element to reflect the capacitive response in a non-ideal state of the interface. The capacitance is used to estimate the passive film thickness [3]. Comparing the experimental data of Table 1, from 0.01 mol/L to 0.05 mol/L of F^{-} and Cl^{-}-containing acidic solution, the values of polarization resistance and capacitance gradually becomes smaller (R_p from 157.83 to 77.18$\mathrm{K\Omega \cdot cm^{-2}}$ and the capacitance from 77.40 to 61.87$\mathrm{\mu F \cdot cm^{-2}}$ in the F^{-}-containing acidic solution; R_p from 210.97 to 135.39 $\mathrm{K\Omega \cdot cm^{-2}}$ and capacitance from 118.00 to 100.59 $\mathrm{\mu F \cdot cm^{-2}}$ in the Cl^{-}-containing acidic solution), and the values of the polarization resistance and capacitance of the sample in the Cl^{-}-containing acidic solution at the same concentration were higher than those in the F^{-}-containing acidic solution. The polarization resistance changes significantly with an increasing concentration of F^{-}, with 36% reduction of R_p in HCl solution but 51% in HF solution, which is an indication that 904L is more sensitive to F^{-}. As the concentration increases, the ability of passive film protection decreases, and the ability of passive film protection formed by 904L in the Cl^{-}-containing acidic solution is better than in the F^{-}-containing acidic solution. It also indicates that the F^{-} has a great influence on the 904L passive film. The above results are in good agreement with the polarization curve.

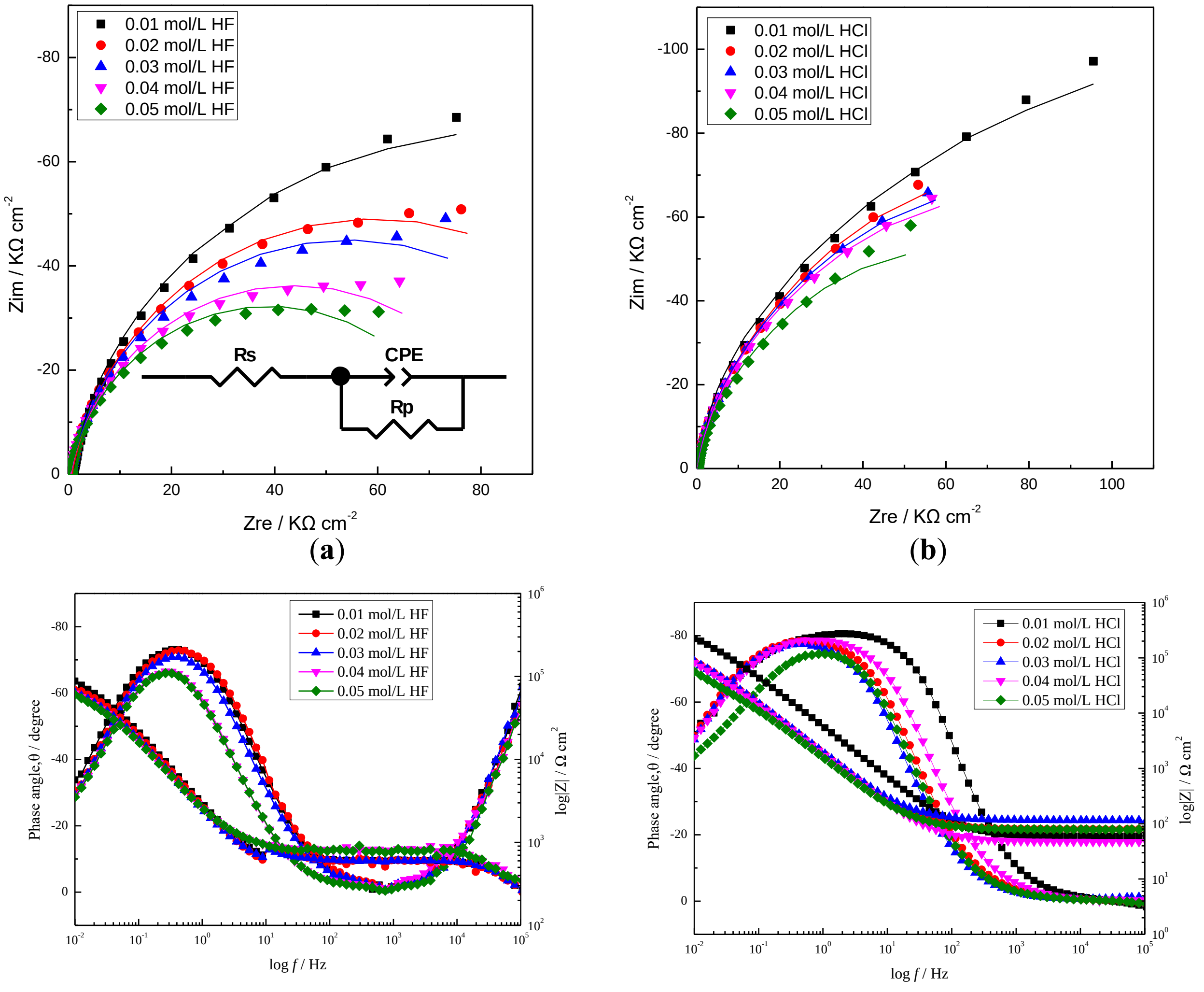

(a) (b)

(c) (d)

Figure 2. Electrochemical impedance spectroscopy (EIS) diagrams of 904L in 0.01–0.05 mol/L (a,c) HF, and (b,d) HCl solution. Nyquist (a,b) and Bode plots (c,d).

Table 3. Results analyzed from EIS.

		Rs (Ω · cm^{-2})	CPE/μF · cm^{-2}	n	Rp/KΩ · cm^{-2}
HF	0.01mol/L	1008±20	77.4±1.5	0.88±0.03	157.83±0.52
	0.02 mol/L	617±15	69.1±2.0	0.89±0.02	117.46±0.41
	0.03 mol/L	490±18	68.2±2.2	0.89±0.02	107.71±0.37
	0.04 mol/L	348±14	64.7±2.5	0.89±0.01	86.76±0.22
	0.05 mol/L	400±25	61.9±3.1	0.89±0.03	77.18±0.34
HCl	0.01 mol/L	202±11	118.0±1.0	0.88±0.01	210.97±0.78
	0.02 mol/L	117±10	107.7±2.1	0.88±0.02	165.69±0.62
	0.03 mol/L	81±8	105.3±1.8	0.89±0.03	156.85±0.54
	0.04 mol/L	60±7	102.8±2.9	0.88±0.01	153.39±0.42
	0.05 mol/L	48±8	100.6±4.2	0.89±0.03	135.39±0.41

3.3. Cyclic Potentiodynamic polarization curve

The pitting nucleation and re-passivation behavior of 904L in the 0.01–0.05 mol/L HF and HCl solutions were characterized by a cyclic potentiodynamic polarization method. As shown in Fig. 3, a significant hysteresis loop appears in the F^--containing acidic solution, and the area of the hysteresis loop increases as the solution concentration increases. In the 0.01 and 0.02 mol/L Cl^--containing acidic solution, however, when the current reaches the peak, it is less than retrace current value, indicating that pit nucleation does not occur at this concentration [21]; a hysteresis loop occurs when the concentration of the Cl^--containing acidic solution is 0.03 mol/L.

Figure. 4 shows the statistical results of breakdown potential (E_{b}), re-passivation potential (E_{rp}), and the solution concentration of Fig. 3. Because the hysteresis loop does not appear in 0.01–0.02mol/L HCl solution, the E_{b} and E_{rp} position is opposite to other concentrations. It shows that the E_{b} of 904L in the Cl^- solution is higher than that of the F^- solution and the difference between the E_{rp} and the E_{b} is small. These results reveal that the passive films formed in Cl^--containing acid solution is significantly less defective and more resistant to film breakdown than those formed on F^--containing acid solution.

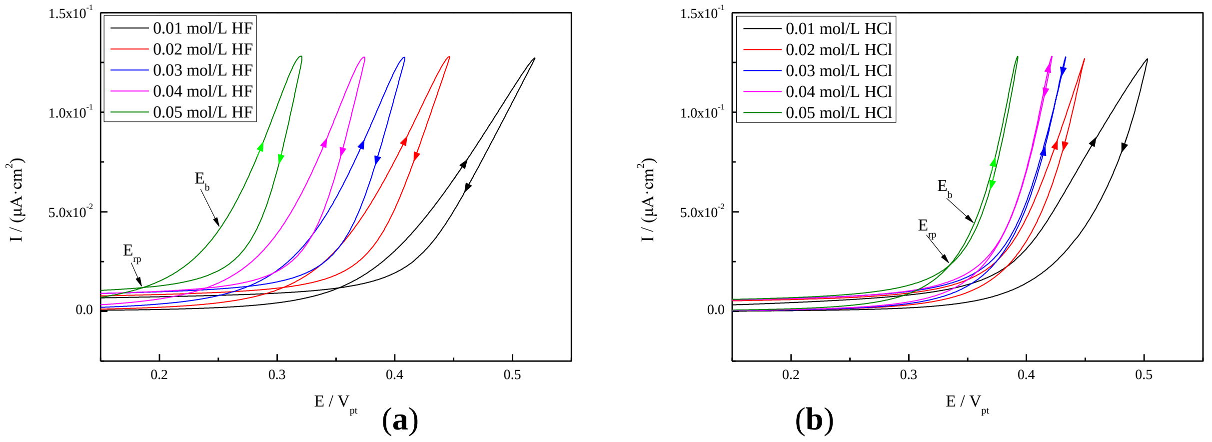

Figure 3. Cyclic potentiodynamic polarization for 904L at 0.01–0.05 mol/L (a) HF, and (b) HCl solution.

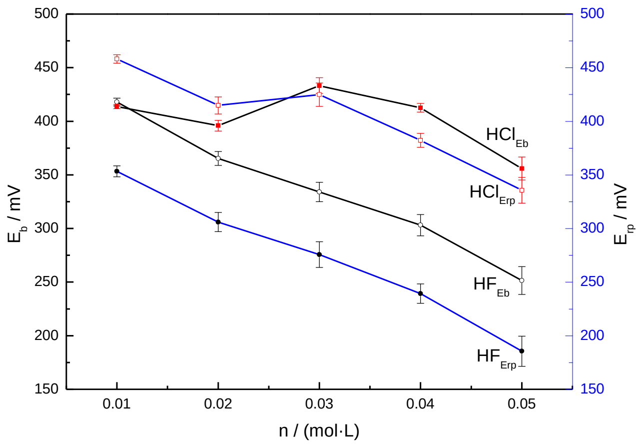

Figure 4. Statistical results of breakdown potential and re-passivation potential and concentration in cyclic polarization curves.

3.4. Potentiostatic polarization curve

The potentiostatic polarization curve of each solution is shown in Fig. 5. This figure reflects the surface dissolution and passive film formation information of 904L stainless steel in each solution. In Fig. 5a,b, the current rapidly decreases with time from the beginning, a phenomenon mainly due to the fact that the passive film nucleation and the growth rate are much faster than the surface dissolution rate of the stainless steel, over time.

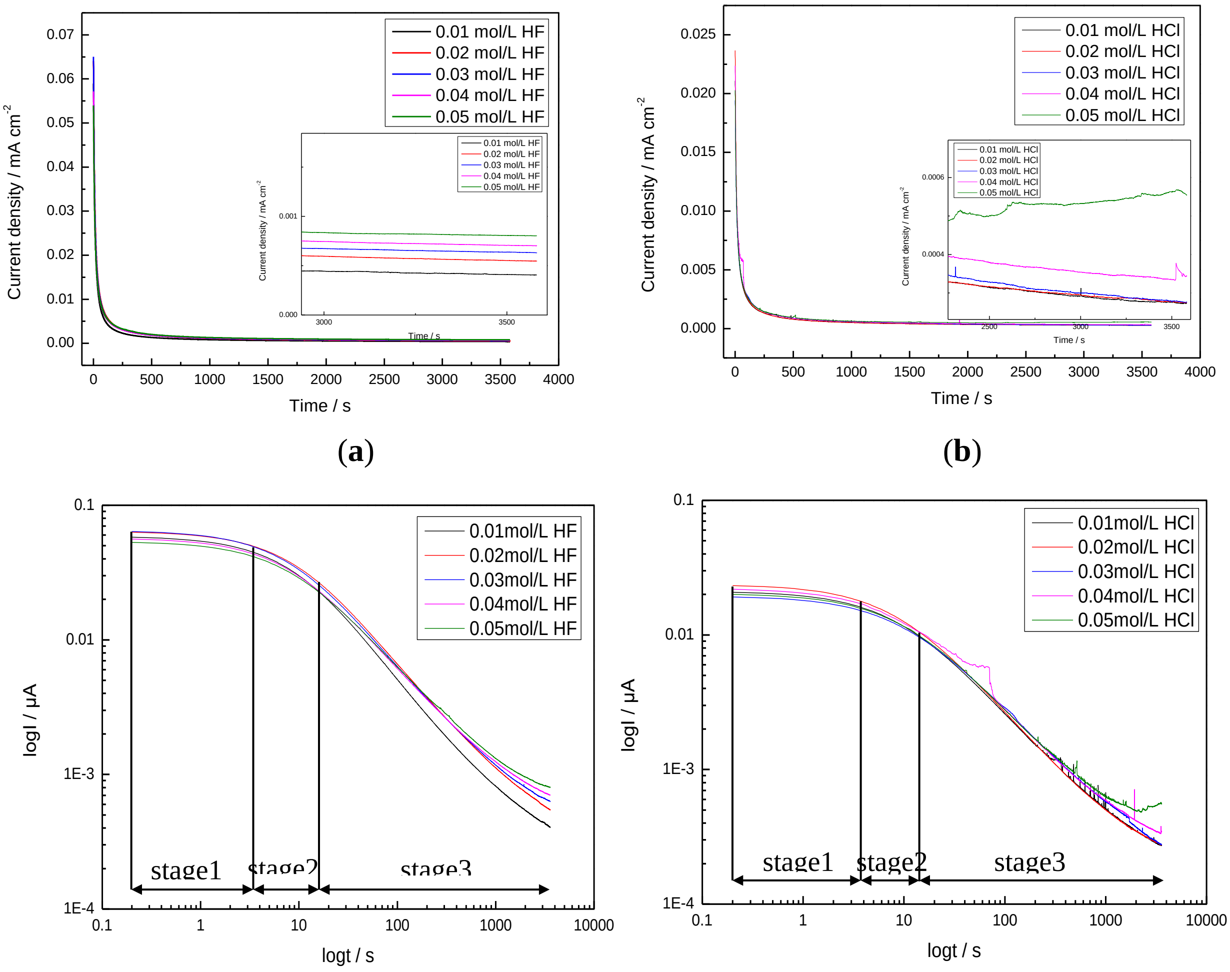

(a) (b)

(c) (d)

Figure 5. (a, b) Current-time transients and (c, d) log i–log t plots of current time for 904L stainless steel in 0.01–0.05 mol/L (a, c) HF, and (b, d) HCl solution.

A relatively stable passive current density (i_{pass}) is gradually formed, which indicates that a completeness of passive film is formed on the surface of the stainless steel. It can be observed that the i_{pass} is increased with the increase in the solution concentration, and the i_{pass} of the F^--containing acidic solution is relatively large, indicating that the passive film formed by the 904L stainless steel in the F^- solution is weak and unstable. Fluoride ion is more aggressive than Cl^-. In Fig. 5a,b, it can be seen from the partial, enlarged view that there is a current fluctuation in the Cl^--containing acidic solution, which indicates formation of metastable pitting and self-repair of the passive film [22–25]. However, it is not present in the F^--containing acidic solution, which also indicates that the two ions' corrosion mechanisms are different.

Escrivà-Cerdán et al. [19,26] used the method of anodic potentiostatic polarization to study the electrochemical behavior of stainless steel in phosphoric acid solution containing impurity ions at different temperatures, which represents the characteristics of different stages of passive film growth. The log i–log t plots of 904L in different concentrations of HF and HCl solutions are given in Fig. 5c,d. The anode transient current is divided into three stages. The anode current in the first stage is constant, meaning that the current is constant due to equilibrium between dissolution and diffusion rate of depolarization agent. The second stage is the transition period, during which the current begins to decrease. In the third stage, the anode current density decreases linearly with time on a logarithmic scale, current density decreases due to the passive film formation rate control the dissolution rate on the exposed surface [27].

3.5. Morphology analysis

As shown in Figure. 6, the pitting morphology of 904Lss after immersion for a different number of days in 200 mL 0.05 mol/L HF and HCl solutions. The pit can be clearly observed on the first day of immersion in the solutions. The pits increase with the immersion time, and there are multiple pits formed into a larger pit (Fig. 6f). It can be observed that pitting corrosion is heavy in the F^--containing acidic solution, Fig. 6b, d and f shows a large amount of white dot-like product enrichment exist around the pit.

Energy dispersive X-ray spectroscopy (EDX) was used to analyze the elements of the films and their rough ranges in the areas marked in Fig. 6e and f, and the results are listed in Table 4. It is observes that the composition of elements inside and outside the pit are different: In the F^--containing acidic solution, the surface of the sample has a low content of Cr and Mo, indicating that the sample is easily been corroded in the F^--containing acidic solution. In the Cl^--containing acidic solution, the amount of Cu element is enriched in the pit and dissolved in the solution.

Corrosion products exist around pits in F^- acidic solution, and corrosion production is gradually enriched with time, having a certain hindrance effect on forming and repairing 904L surface passive film, thereby further destroying the integrity of the passive film, forming pitting nucleation sites, and growing upwards, eventually forming a steady-state pit [1]. Therefore, in the same conditions, the destructive ability of F^- in relation to 904L surface passive film is greater than Cl^-, which echoes previous electrochemical information. In other studies [6,7], it is also mentioned that F^- and Cl^- are two different types of ions, and F^- is easily adsorbed onto the surface of the sample to form a F^--containing corrosion product, thereby hindering the formation of a passive film; thus pitting is formed. The Cl^- tends to penetrate the surface of passive film arriving at the substrate through the defect, and the concentration continues to increase until the passive film breakdown.

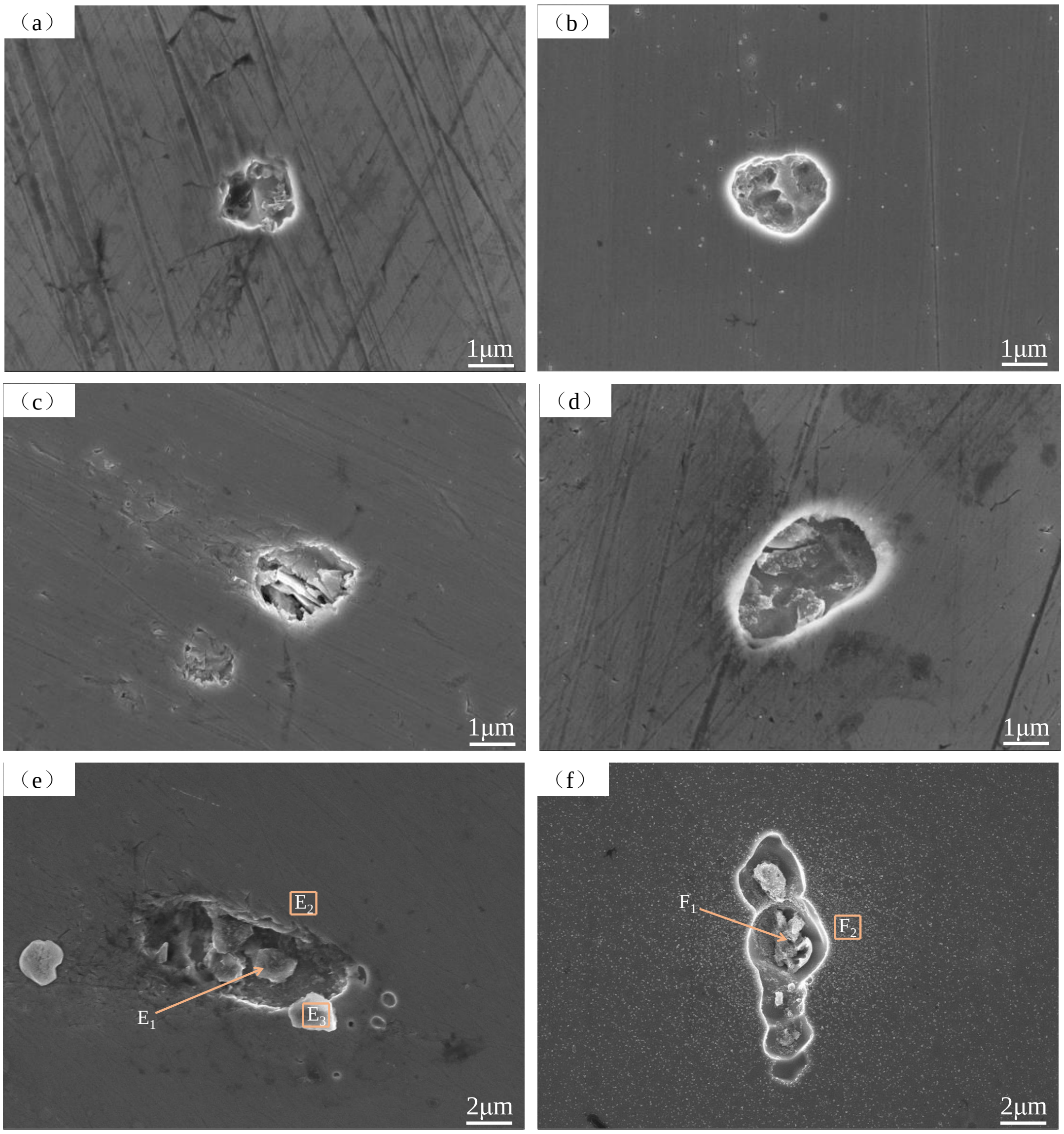

Figure 6. Local corrosion morphology of 904L surface after immersion in 0.01–0.05 mol/L HCl for one day (a), seven days (c), and fifteen days (e); and 0.01–0.05 mol/L HF of one day (b), seven days (d), and fifteen days (f).

Table 4. EDX results of the regions marked in Fig. 6 (wt%).

Elements	E1	E2	E3	F1	F2
Cl	0.33	-	0.20	-	-
F	-	-	-	12.89	1.06
Cr	22.39	20.73	21.40	18.10	19.56
Ni	11.86	23.21	18.42	18.98	23.91
Fe	35.51	46.05	40.05	39.94	46.13
Mn	1.18	1.52	0.93	1.28	1.41
Cu	18.94	3.19	12.01	2.97	2.97
Mo	9.36	4.62	6.54	5.84	4.46
Co	0.43	0.64	0.45	-	0.5

3.6. Surface characterization

In order to compare the effects of F^- and Cl^- on the composition of 904Lss passive film, the XPS test was carried out on the surface passive film of 904Lss after immersion for seven days in 0.05 mol/L HF and HCl solution. Fig. 7 shows the results of the XPS spectra. It shows that the surface passive film not only has peaks of Mo3d, O1s, Cr2p, Mn2p, Fe2p, and Ni2p after seven days of F^- immersion but also has peaks of F1s and Cu2p. It is observed that F1s exists in the passive film of the sample immersed in F^--containing acidic solution, indicating that F^- participates in the composition of the passive film [5]; so, the experimental data of the polarization curve and EIS have been confirmed.

The presence of F^--containing compound on the surface of the sample hinders the self-repair of the passive film, reduces the integrity of the passive film, the initiation point of pitting occurs, and a large cathode and small anode phenomenon is formed, which further accelerates the destruction of the passive film. However, the sample immersed in the Cl^--containing acidic solution has a selective dissolution behavior, which first reacts preferentially with Cu on the surface of the sample; thus, stable and beneficial elements of the passive film are consumed by Cr, Ni, and so on, thereby reducing the likelihood of the passive film's destruction and improving the stability of the passive film.

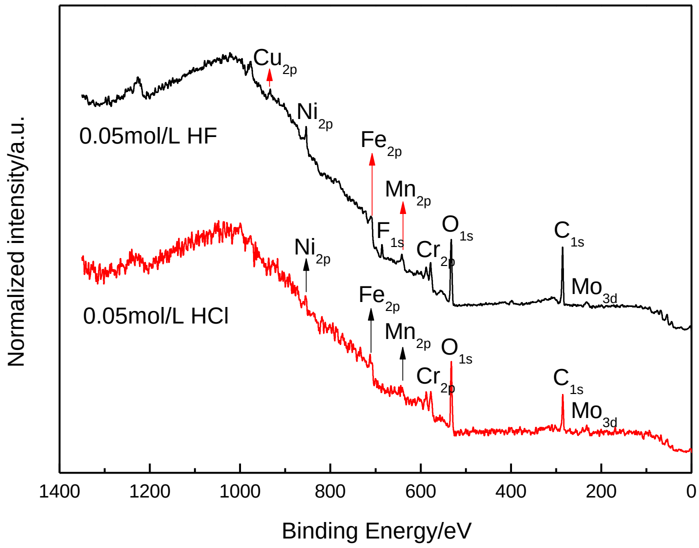

Figure 7. XPS survey scan acquired from the outermost surfaces of the 904L samples after immersion in 0.05mol/L HF and HCl solution at 25°C for 7 days.

Figure.8 shows a high-resolution XPS spectrum of Mo3d, Cr2p3/2, Ni2p3/2, and Mn2p3/2. Compared with the solution after immersion for seven days in the Cl^--containing acidic solution, the low content of Mo^{x+} on the surface of the passive film, and Mo^{x+} has the effect of blocking F^- and Cl^- corroded [28–30]. The content of Cr_2O_3 and $Cr_2(OH)_3$ is dominant in Cr2p3/2, but there is more Cr_2O_3 content in the passive film after immersion in Cl^--containing acidic solution. The Cr_2O_3 has a positive impact on the stability of the passive film. In the F^--containing acidic solution, there is more of the Ni metal state and less of the Ni oxidation state and the hydroxide state. According to two studies [31,32], the outer layer of the passive film is mainly composed of the Fe–Ni oxidation state and the Ni hydroxide state. Therefore, the stability of the passive film in the F^--containing acidic solution is worse than that in the Cl^--containing acidic solution.

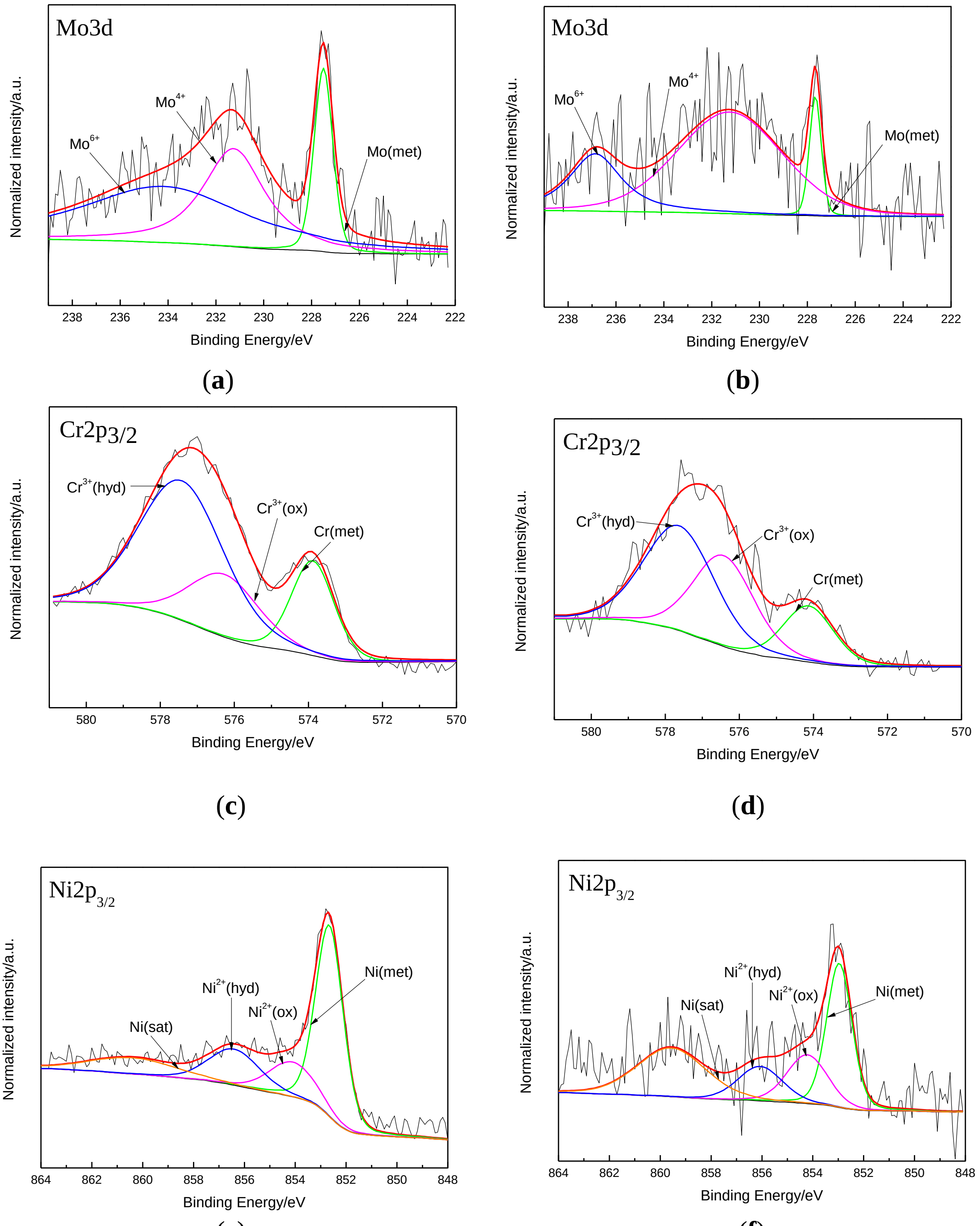

(a) **(b)**

(c) **(d)**

(e) **(f)**

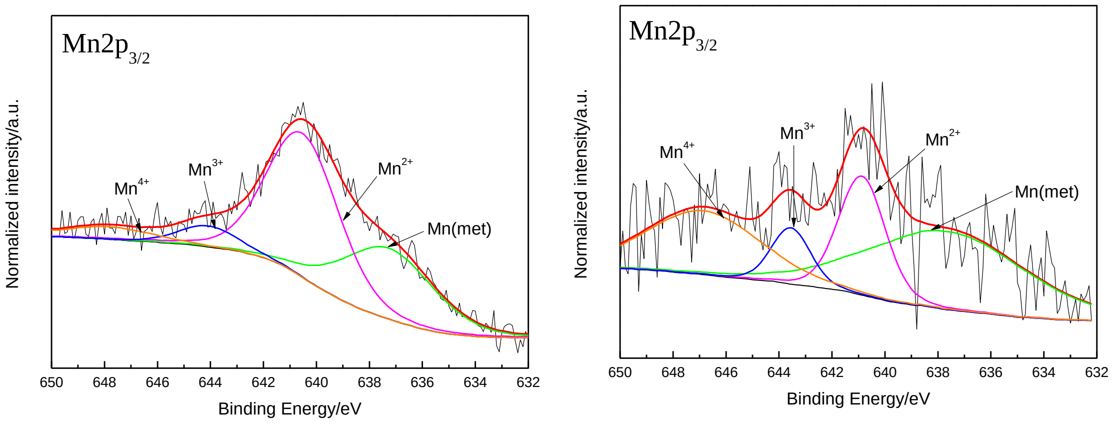

(g) **(h)**

Figure 8. XPS regional scan acquired from the outermost surfaces of the 904L samples after immersion in 0.05 mol/L HF and HCl solution at 25℃ for 7 days. The spectra correspond to (a,b) Mo3d, (c,d) $Cr2p_{3/2}$, (e,f) $Ni2p_{3/2}$, and (g,h) $Mn2p_{3/2}$.

The manganese oxide content of the surface of the passive film formed in the F^--containing acidic solution is higher than that of the passive film formed in the Cl^--containing acidic solution, and some studies have shown that the presence of manganese oxide in the passive film is reduced. It can improve the stability of the passive film and has better corrosion resistance [33–35]. Due to the low Mo^{x+}, Cr_2O_3, Ni oxidation state and hydroxide state content and high manganese oxide content, the F^--induced 904L passive film has poor stability and is easy destroyed, which is not conducive to the long-term survival of the material in a service environment.

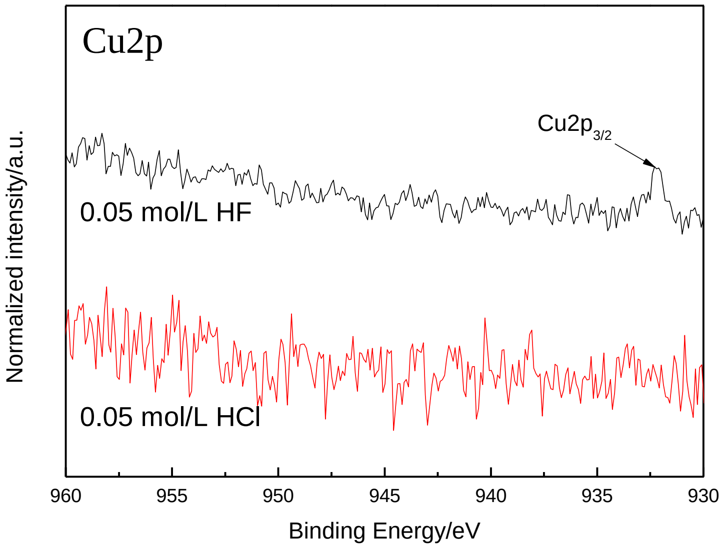

Figure 9. XPS regional scan acquired from the outermost surfaces of the 904L samples after immersion in 0.05mol/L HF and HCl solution at 25℃ for 7 days. The spectra correspond to Cu2p.

Figure 9 presents the XPS spectrum of Cu2p. It can be seen from the figure that $Cu_{(met)}$ (933eV) exists on the surface of the passive film formed in the F⁻-containing acid solution, indicating that the copper element participates in the composition of the passive film, but in the Cl⁻-containing solution, no copper peak is found on the surface of the passive film. Therefore, it can be considered that the Cl⁻-containing acidic solution has a preferential dissolution behavior for the copper element in 904L, so that the consumption of Cr, Ni, and Mo is reduced, and the stability of the passive film structure is further improved, and the enrichment of Cl⁻ at the passive film-matrix interface is hindered, improving the corrosion resistance of 904L in Cl⁻-containing acidic solution.

Therefore, it can be concluded from the XPS information in Fig. 8 and Fig. 9 that the structure of passive film formed in the Cl⁻-containing acidic solution is superior to the passive film formed in the F⁻-containing acidic solution.

Figure 10a shows the concentration obtained by inductively coupled plasma optical emission spectrometer (ICP-OES) analysis of the solution medium after immersion in 0.05 mol/L HF and HCl for seven days, and Fig. 10b shows the comparison of the mass percentage of each element of the original 904L and its solution after immersion for seven days in 0.05 mol/L HF and HCl at room temperature. It can be seen from Fig. 10a that the content of the eluted elements of Cr, Ni, Mo, and Mn are much higher in the F⁻-containing acidic solution than in the Cl⁻-containing acidic solution, but the Cu element content is opposite.

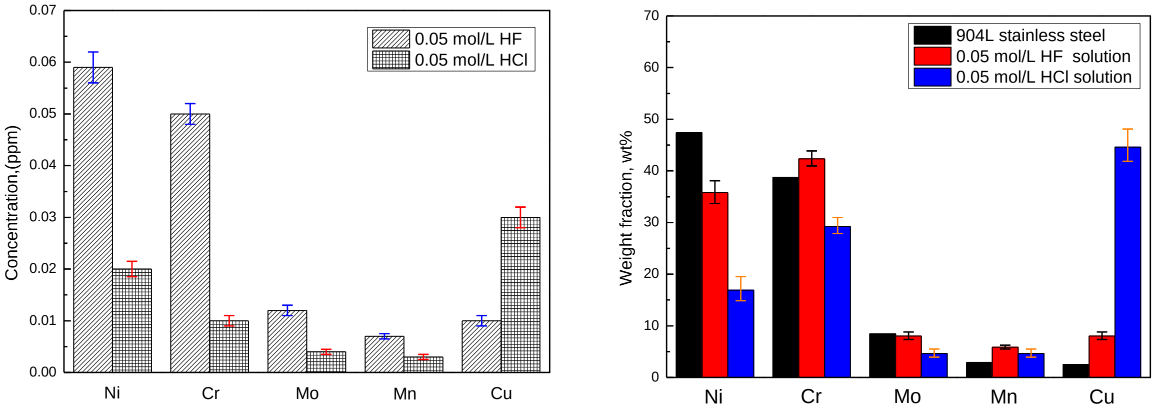

(**a**) (**b**)

Figure 10. Percentage of cation in solution of 904L samples after immersion in 0.05 mol/L HF and HCl solution at 25°C for 7 days; comparison of elemental weight fraction of 904L and its solution after immersion in 0.05 mol/L HF, HCl for seven days at 25°C.

It shows that the 904L stainless steel has poor corrosion resistance in the F⁻-containing acidic solution, and the 904L stainless steel preferentially dissolves the Cu element in the Cl⁻-containing acidic solution. Fig. 10b shows that the mass fraction of Cr, Mo, and Cu in the F⁻-containing acidic solution is high, and the mass fraction of Cu in the Cl⁻-containing acidic solution accounts for a large proportion, being 17.8 times the original 904L and 5.6 times the F⁻-containing acidic solution. This indicates that the amount of Cu dissolved in the Cl⁻-containing acidic solution is large, and the composition of the Cr and Ni elements is more involved in the passive film; in the F⁻-containing acidic solution, the Cr element is better dissolved, so that the passive film component lacks the Cr element. The 904L is poorly self-passivating in the solution [36], and the structure of passive film is less stable than in the Cl⁻-containing acidic solution and tends to erode the material. The results are in good agreement with the above polarization curves, EIS and XPS analysis results.

The present results show the different passive films formed by 904L stainless steel in two different ionic solutions. Fig. 11 presents a schematic, which can explain the differences. Firstly, when the specimen makes contact with the acid medium, the oxidation layer of the 904L is breakdown and the substrate material is exposed to corrosive media and is attacked by F⁻ and Cl⁻. However, this was observed to a lesser extent for Cl⁻-containing acidic solution with a Cr element (Fig. 10b). Consequently, the Cl⁻ preferentially dissolves the Cu element and does not participate in the composition of the re-passivation (Fig. 11b), whereas the F⁻ participates in the composition of the re-passivation (Fig. 11a). Therefore, according to the results of XPS, the content of Cr and Ni in the re-passivation film formed in the F⁻-containing acidic solution was decreased. (Fig. 8 and 9).

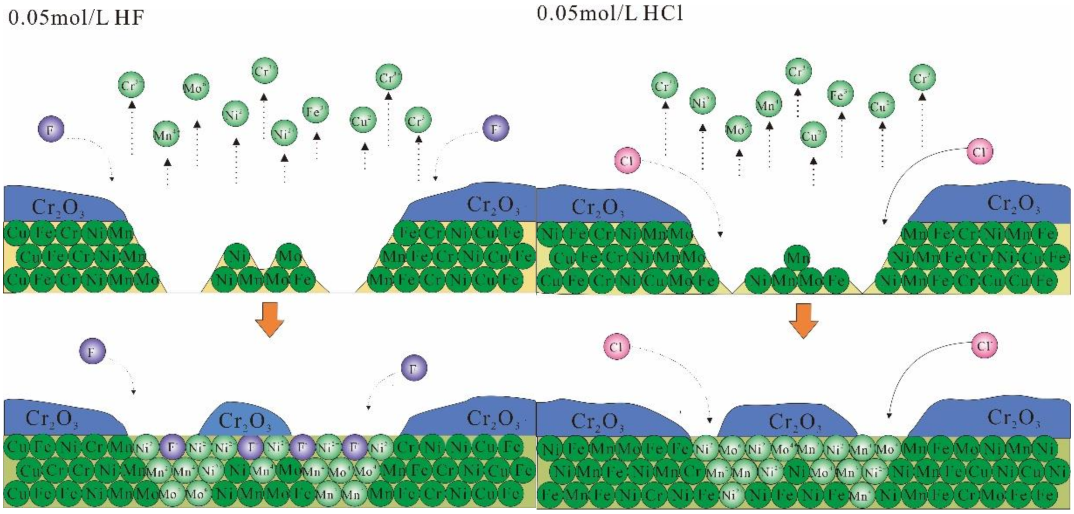

(a) **(b)**

Figure 11. Schematic representation of the evolution of passivation film of 904L stainless steel after immersion in 0.05 mol/L HF (a) and HCl (b) at room temperature.

4. CONCLUSIONS

The difference between F⁻ and Cl⁻ in the corrosion process is mainly due to the different mechanisms of re-passivation. According to the hysteresis of the cyclic polarization curve, a large hysteresis loop appears in the HF solution, the hysteresis loop is related to the diffusion and migration of F⁻ on the passivation film.

XPS analysis shows that 904L austenitic stainless steel in the F^--concentration acidic solution, the surface of the re-passivation film has a low content of Mo^{x+}, Cr_2O_3, Ni oxidation state and hydroxide state, and a high content of manganese oxide, meanwhile, the F^- participated in the composition of the 904L re-passivation. Which make 904L high passivation current, a significant hysteresis loop, and more susceptible to erosion.

ACKNOWLEDGMENTS
We gratefully acknowledge the financial assistance of the National Natural Science Foundation of China (Grant Nos. 51661006, 51774103, and 51974097), the Program of "One Hundred Talented People" of Guizhou Province (Grant No. 20164014), the Guizhou Province Science and Technology Project (Grant Nos. 20175656, 20175788, 20191414, and 20192162), and the Program for Innovation Research Team of Guizhou Province Education Ministry (Grant No. 2016021).

References

1. D.D. Macdonald, *J. Electrochem. Soc.*, 139 (1992) 3434.
2. Z. Szklarska-Smialowska, *Corros. Sci.*, 44 (2002) 1143.
3. Y.X. Qiao, Y.G. Zheng, W. Ke and P.C. Okafor, *Corros. Sci.*, 51 (2009) 979.
4. B. Zhang, J. Wang, B. Wu, X.W. Guo, Y.J. Wang, D. Chen, Y.C. Zhang, K. Du, E.E. Oguzie and X.L. Ma, *Nat. Commun.*, 9 (2018) 2559.
5. G.B. Zou, W. Shi, S. Xiang, X.M. Ji, G.Q. Ma and R.G. Ballinger, *RSC Adv.*, 8 (2018) 2811.
6. J.L. Trompette, L. Massot, L. Arurault and S. Fontorbes, *Corros. Sci.*, 53 (2011) 1262.
7. J.L. Trompette, L. Arurault, S. Fontorbes and L. Massot, *Electrochim. Acta*, 55 (2010) 2901.
8. M.C. Li, C.L. Zeng, H.C. Lin and C.N. Cao, *Br. Corros. J.*, 36 (2001) 179.
9. T. Bellezze, G. Giuliani, G. Roventi, R. Fratesi, F. Andreatta and L. Fedrizzi, *Mater. Corros.*, 67 (2016) 831.
10. I.S. Molchan, G.E. Thompson, J. Walton, P. Skeldon, A. Tempez and S. Legender, *Appl. Surf. Sci.*, 357 (2015) 37.
11. H. Iken, R. Basseguy, A. Guenbour and A.B. Bachir, *Electrochim. Acta*, 52 (2007) 2580.
12. H.H. Strehblow and B. Titze, *Corros. Sci.*, 17 (1977) 461.
13. C.A.D. Rovere, J.H. Alano, R. Silva, P.A.P. Nascente, J. Otubo and S.E. Kuri, *Corros. Sci.*, 57 (2012) 154.
14. G. Tranchida, M. Clesi, F.D. Franco, F.D. Quarto and M. Santamaria, *Electrochim. Acta*, 273 (2018) 412.
15. G. Capobianco, G. Sandona, T. Monetta and F. Bellucci, *Corros. Sci.*, 35 (1993) 35.
16. S. Fajardo, D.M. Bastidas, M. Criado and J.M. Bastidas, *Electrochim. Acta*, 129 (2014) 160.
17. H. Luo, Z. Li, A.M. Mingers and D. Raabe, *Corros. Sci.*, 134 (2018) 131.
18. V. Feliu, J.A. Gonzalez, C. Andrade and S. Feliu, *Corros. Sci.*, 40 (1998) 975.
19. C. Escrivà-Cerdán, E. Blasco-Tamarit, D.M. García-García, J. García-Antón and A. Guenbour, *Corros. Sci.*, 56 (2012) 114.
20. N.E. Hakiki, S. Boudin, B. Rondot and M.D.C. Belo, *Corros. Sci.*, 37 (1995) 1809.
21. A. Poursaee, *Electrochim. Acta*, 55 (2010) 1200.
22. Y. Miyata, T. Handa and H. Takazawa, *Corros. Sci.*, 31 (1990) 465.
23. G.O. Ilevbare and G.T. Burstein, *Corros. Sci.*, 43 (2001) 485.
24. F. Eghbali, M.H. Moayed, A. Davoodi and N. Ebrahimi, *Corros. Sci.*, 53 (2011) 513.
25. Z. Wang, Z.Q. Zhou, L. Zhang, J.Y. Hu, Z.R. Zhang and M.X. Lu, Acta Metall. Sinica, 32 (2018) 585.

26. C. Escrivà-Cerdán, E. Blasco-Tamarit, D.M. García-García, J. García-Antón, R. Akid and J. Walton, *Electrochim. Acta*, 111 (2013) 552.
27. S.I. Pyun and E.J. Lee, *Electrochim. Acta*, 40 (1995) 1963.
28. Y. Li, X. Fan, N. Tang, H. Bian, Y. Hou, Y. Koizumi and A. Chiba, *Corros. Sci.*, 78 (2014) 101.
29. A. Pardo, M.C. Merino, A.E. Coy, F. Viejo, R. Arrabal and E. Matykina, *Corros. Sci.*, 50 (2008) 780.
30. H. Habazaki, A. Kawashima, K. Asami and K. Hashimoto, *Corros. Sci.*, 33 (1992) 225.
31. L. Marchetti, F. Miserque, S. Perrin and M. Pijolat, *Surf. Interface Anal.*, 47 (2015) 632.
32. F. Delabrouille, B. Viguier, L. Legras and E. Andrieu, *Mater. High Temp.*, 22 (2005) 287.
33. Y.S. Zhang and X.M. Zhu, *Corros. Sci.*, 41 (1999) 1817.
34. K.M. Moon, D.A. Kim, Y.H. Kim and M.H. Lee, *Int. J. Mod. Phys. B*, 32 (2018) 1840083.
35. H. Luo, Z. Li, A.M. Mingers and D. Raabe, *Corros. Sci.*, 134 (2018) 131.
36. C.O.A. Olsson and D. Landolt, *Electrochim. Acta*, 48 (2003) 1093.